The Berkeley Lower Extremity Exoskeleton

H. Kazerooni

R. Steger
e-mail: exo@berkeley.edu

University of California, Berkeley,
Berkeley, CA 94720

The first functional load-carrying and energetically autonomous exoskeleton was demonstrated at the University of California, Berkeley, walking at the average speed of 1.3 m/s (2.9 mph) while carrying a 34 kg (75 lb) payload. Four fundamental technologies associated with the Berkeley lower extremity exoskeleton were tackled during the course of this project. These four core technologies include the design of the exoskeleton architecture, control schemes, a body local area network to host the control algorithm, and a series of on-board power units to power the actuators, sensors, and the computers. This paper gives an overview of one of the control schemes. The analysis here is an extension of the classical definition of the sensitivity function of a system: the ability of a system to reject disturbances or the measure of system robustness. The control algorithm developed here increases the closed-loop system sensitivity to its wearer's forces and torques without any measurement from the wearer (such as force, position, or electromyogram signal). The control method has little robustness to parameter variations and therefore requires a relatively good dynamic model of the system. The trade-offs between having sensors to measure human variables and the lack of robustness to parameter variation are described. [DOI: 10.1115/1.2168164]

1 Introduction

The primary objective of the Berkeley Lower Extremity Exoskeleton (BLEEX) Project at the University of California, Berkeley is to develop fundamental technologies associated with the design and control of energetically autonomous lower extremity exoskeletons that augment human strength and endurance during locomotion. The first field-operational lower extremity exoskeleton is comprised of two powered anthropomorphic legs, a power unit, and a backpack-like frame on which a variety of heavy loads can be mounted. This system provides its pilot (i.e., the wearer) the ability to carry significant loads on his/her back with minimal effort over any type of terrain. BLEEX allows the pilot to comfortably squat, bend, swing from side to side, twist, and walk on ascending and descending slopes, while also offering the ability to step over and under obstructions while carrying equipment and supplies. Because the pilot can carry significant loads for extended periods of time without reducing his/her agility, physical effectiveness increases significantly with the aid of this class of lower extremity exoskeletons. In order to address issues of field robustness and reliability, BLEEX is designed such that, in the case of power loss (e.g. from fuel exhaustion), the exoskeleton legs can be easily removed and the remainder of the device can be carried like a standard backpack.

BLEEX was first unveiled in 2004, at the University of California, Berkeley's Human Engineering and Robotics Laboratory (Fig. 1) [1–3]. In this initial model, BLEEX offered a carrying capacity of 34 kg (75 lb), with weight in excess of that allowance being supported by the pilot. BLEEX's unique design offers an ergonomic, highly maneuverable, mechanically robust, lightweight, and durable outfit to surpass typical human limitations. BLEEX has numerous potential applications; it can provide soldiers, disaster-relief workers, wildfire fighters, and other emergency personnel the ability to carry heavy loads, such as food, rescue equipment, first-aid supplies, communications gear, and weaponry, without the strain typically associated with demanding labor. It is our vision that BLEEX will provide a versatile and realizable transport platform for mission-critical equipment.

The capability of the lower extremity exoskeleton stems from the combined benefit of the human intellect provided by the pilot and the strength advantage offered by the exoskeleton; in other words, the human provides an intelligent control system for the exoskeleton while the exoskeleton actuators provide most of the strength necessary for walking. The control algorithm ensures that the exoskeleton moves in concert with the pilot with minimal interaction force between the two. The control scheme needs no direct measurements from the pilot or the human-machine interface (e.g., no force sensors between the two); instead, the controller estimates, based on measurements from the exoskeleton only, how to move so that the pilot feels very little force. This control scheme, which has never before been applied to any robotic system, is an effective method of generating locomotion when the contact location between the pilot and the exoskeleton is unknown and unpredictable (i.e., the exoskeleton and the pilot are in contact in a variety of places). This control method differs from compliance control methods employed for upper extremity exoskeletons [4–6] and haptic systems [7,8] because it requires no force sensor between the wearer and the exoskeleton.

The basic principle for the control of BLEEX rests on the notion that the exoskeleton needs to shadow the wearer's voluntary and involuntary movements quickly, and without delay. This requires a high level of sensitivity in response to all forces and torques on the exoskeleton, particularly, the forces imposed by the pilot. Addressing this need involves a direct conflict with control science's goal of minimizing system sensitivity in the design of a closed-loop feedback system. If fitted with a low sensitivity, the exoskeleton would not move in concert with its wearer. We realize, however, that maximizing system sensitivity to external forces and torques leads to a loss of robustness in the system.

Taking into account this new approach, our goal was to develop a control system for BLEEX with high sensitivity. We were faced with two realistic concerns; the first was that an exoskeleton with high sensitivity to external forces and torques would respond to other external forces not initiated by its pilot. For example, if someone pushed against an exoskeleton that had high sensitivity, the exoskeleton would move the same way it would move in response to the forces from its pilot. Although the fact that it does not stabilize its behavior on its own in response to other forces

Contributed by the Dynamic Systems Division of ASME for publication in the JOURNAL OF DYNAMIC SYSTEMS, MEASUREMENT, AND CONTROL. Manuscript received March 31, 2005; final manuscript received September 17, 2005. Assoc. Editor: Sunil K. Agrawal. Paper presented at the IEEE Robotics and Automation Conference 2005.

Fig. 1 Berkeley lower extremity exoskeleton (BLEEX) and pilot Ryan Steger. (1) Load occupies the upper portion of the backpack and around the power unit, (2) rigid connection of the BLEEX spine to the pilot's vest, (3) power unit and central computer occupies the lower portion of the backpack, (4) semi-rigid vest connecting BLEEX to the pilot, (5) one of the hydraulic actuators, and (6) rigid connection of the BLEEX feet to the pilot's boots (more photographs can be found at http://bleex.me.berkeley.edu).

may sound like a serious problem; if it did (e.g., using a gyro), the pilot would receive motion from the exoskeleton unexpectedly and would have to struggle with it to avoid unwanted movement. The key to stabilizing the exoskeleton and preventing it from falling in response to external forces depends on the pilot's ability to move quickly (e.g., step back or sideways) to create a stable situation for himself and the exoskeleton. For this, a sufficiently wide control bandwidth is needed so the exoskeleton can respond to both pilot's voluntary and involuntary movements (i.e., reflexes).

The second concern is that systems with high sensitivity to external forces and torques are not robust to variations, and therefore, the precision of the system performance will be proportional to the precision of the exoskeleton dynamic model. Although this is a serious drawback, we have accepted it as unavoidable. Nevertheless, various experimental systems in our laboratory have proved the overall effectiveness of the control method in shadowing the pilot's movement.

2 Previous Work

In the early 1960s, the U.S. Defense Department expressed interest in the development of a man-amplifier, a "powered suit of armor" that would augment soldiers' lifting and carrying capabilities. In 1962, the U.S. Air Force had the Cornell Aeronautical Laboratory study the feasibility of using a master-slave robotic system as a man-amplifier. In later work, Cornell determined that an exoskeleton—an external structure in the shape of the human body that has far fewer degrees of freedom than a human—could accomplish most desired tasks [9]. From 1960 to 1971, General Electric developed and tested a prototype man-amplifier, a master-slave system, called the Hardiman [10–13]. The Hardiman was a set of overlapping exoskeletons worn by a human operator. The outer exoskeleton (the slave) followed the motions of the inner exoskeleton (the master), which followed the motions of the human operator. These studies found that duplicating all human motions and using master-slave systems were not practical. Additionally, difficulties in human sensing and system complexity kept it from walking.

Several exoskeletons were developed at the University of Belgrade in the 1960s and 1970s to aid people with paraplegia resulting from spinal cord injury [14,15]. Although these early devices were limited to predefined motions and had limited success, balancing algorithms developed for them are still used in many bipedal robots [16]. Current commercially available rehabilitation devices, such as the "Locomat," use a similar predefined motion strategy to train muscles and nerve pathways for patients with locomotion impairment [17]. The "RoboKnee" is a powered knee brace developed by MIT that functions in parallel to the wearer's knee and transfers load to the wearer's ankle (not to the ground) [18]. "HAL" is an orthosis developed by the University of Tsukuba in Japan that is connected to the patient's thighs and shanks and moves the patient's legs as a function of the EMG signals measured from the wearer [19,20].

In our research work at Berkeley, we have separated the technology associated with human power augmentation into lower extremity exoskeletons and upper extremity exoskeletons. The reason for this was twofold; first, we could envision a great many applications for either a stand-alone lower or upper extremity exoskeleton in the immediate future. Second, and more importantly for the division, is that the exoskeletons are in their early stages, and further research still needs to be conducted to ensure that the upper and lower extremity exoskeletons can function well, independently, before we can venture an attempt to integrate them. With this in mind, we proceeded with the designs of the lower and upper extremity exoskeletons separately, with little concern for the development of an integrated exoskeleton. We will first give a summary of the upper extremity exoskeleton efforts at Berkeley and then will proceed with the description of the BLEEX project.

In the mid-1980s, we initiated several research projects on upper extremity exoskeleton systems, so-called human extenders [4,5,21]. The main function of an upper extremity exoskeleton is human power augmentation for manipulation of heavy and bulky objects. These systems, which are also known as assist devices or human power extenders, can simulate forces on a worker's arms and torso. These forces differ from and are usually much less than the forces needed to maneuver a load. When a worker uses an upper extremity exoskeleton to move a load, the device bears the bulk of the weight by itself, while transferring to the user as a natural feedback, a scaled-down value of the load's actual weight. For example, for a 20 kg (44 lb) object, a worker might support only 2 kg (4.4 lb) while the device supports the remaining 18 kg (39.6 lb). In this fashion, the worker can still sense the load's weight and judge his/her movements accordingly, but the force he/she feels is much smaller than what he/she would feel without

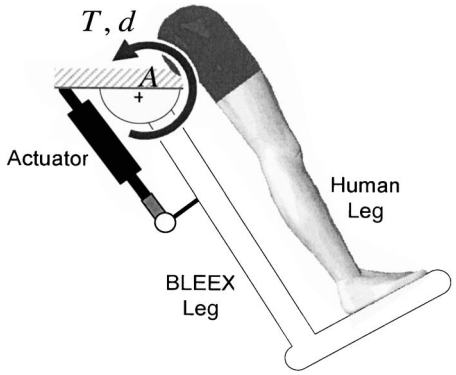

Fig. 2 Simple 1-DOF exoskeleton leg interacting with the pilot leg. The exoskeleton leg has an actuator that produces a torque *T* about the pivot point *A*. The total equivalent torque associated with all forces and torques from the pilot on the exoskeleton is represented by *d*.

the device. In another example, suppose the worker uses the device to maneuver a large, rigid, and bulky object, such as an exhaust pipe in an automotive assembly line. The device will convey the force to the worker as if it was a light, single-point mass. This limits the cross-coupled and centrifugal forces that increase the difficulty of maneuvering a rigid body and can sometimes produce injurious forces on the wrist. In a third example, suppose a worker uses the device to handle a powered torque wrench. The device will decrease and filter the forces transferred from the wrench to the worker's arm so the worker feels the low-frequency components of the wrench's vibratory forces instead of the high-frequency components that produce fatigue.

The Berkeley lower extremity exoskeleton (BLEEX) is not an orthosis or a brace; unlike the above systems, it is designed to carry a heavy load by transferring the load weight to the ground (not to the wearer). BLEEX has four new features. First, a novel control architecture was developed that controls the exoskeleton through measurements of the exoskeleton itself [2]. This eliminated problematic human-induced instability due to sensing the human force [8]. Second, a series of high specific-power and specific-energy power supplies were developed that were small enough to make BLEEX a true field-operational system [22–24]. Third, a body LAN (local area network) with a special communication protocol and hardware was developed to simplify and reduce the cabling task for the sensors and actuators needed for exoskeleton control [25,26]. Finally, a flexible and versatile mechanical architecture was chosen to decrease complexity and power consumption [3]. This paper focuses on the control architecture and gives an overview of the electronic design and the biomimetic mechanical design of the exoskeleton. For further depth in each of these four areas, the reader is referred to the publications referenced above.

3 Controller Description

3.1 A Simple One-Degree-of-Freedom (1-DOF) Example. The control of the exoskeleton is motivated here through the simple 1-DOF example shown in Fig. 2. This figure schematically depicts a human leg attached or interacting with a 1-DOF exoskeleton leg in a swing configuration (no interaction with the ground). For simplicity, the exoskeleton leg is shown as a rigid link pivoting about a joint and powered by a single actuator. The exoskeleton leg in this example has an actuator that produces a torque about pivot point A.

Although the pilot is attached securely to the exoskeleton at the foot, other parts of the pilot leg, such as the shanks and thighs, can contact the exoskeleton and impose forces and torques on the exoskeleton leg. The location of the contacts and the direction of the contact forces (and sometimes contact torques) vary and are

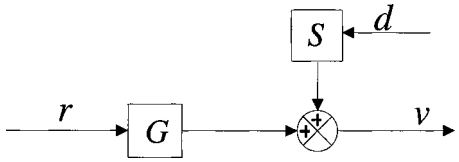

Fig. 3 The exoskeleton's angular velocity is shown as a function of the input to the actuators and the torques imposed by the pilot onto the exoskeleton

therefore considered unknown values in this analysis. In fact, one of the primary objectives in designing BLEEX was to ensure a pilot's unrestricted interaction with it. The equivalent torque on the exoskeleton leg resulting from the pilot's applied forces and torques is represented by d.

In the absence of gravity, (1) and the block diagram of Fig. 3 represent the dynamic behavior of the exoskeleton leg regardless of any kind of internal feedback the actuator may have

$$v = Gr + Sd \tag{1}$$

where G represents the transfer function from the actuator input r to the exoskeleton angular velocity v (actuator dynamics are included in G). In the case where multiple actuators produce controlled torques on the system, $\mathbf{r}$ is the vector of torques imposed on the exoskeleton by the actuators. The form of G and the type of internal feedback for the actuator is immaterial for the discussion here. Also bear in mind the omission of the Laplace operator in all equations for the sake of compactness.

The exoskeleton velocity, as shown by (1), is affected by forces and torques from its pilot. The sensitivity transfer function, S, represents how the equivalent human torque affects the exoskeleton angular velocity. S maps the equivalent pilot torque d onto the exoskeleton velocity v. If the actuator already has some sort of primary stabilizing controller, the magnitude of S will be small and the exoskeleton will only have a small response to the imposed forces and torques from the pilot or any other source. For example, a high-gain velocity controller in the actuator results in small S and consequently a small exoskeleton response to external forces and torques. Also, non-back-drivable actuators (e.g., large transmission ratios or servovalves with overlapping spools) result in a small S, which leads to a correspondingly small response to pilot forces and torques.

Note that d (resulting torque from pilot on the exoskeleton) is not an exogenous input; it is a function of the pilot dynamics and variables, such as position and velocity of the pilot and the exoskeleton legs. These dynamics change from person to person and within a person as a function of time and posture. We will add these dynamics to our analysis later in the paper, but it is unrelated to the purpose of current discussion. We also assume that d is only from the pilot and does not include any other external forces and torques.

The objective is to increase exoskeleton sensitivity to pilot forces and torques through feedback but *without* measuring d. In other words, we are interested in creating a system that allows the pilot to swing the exoskeleton leg easily. Measuring d to create such systems develops several hard, but ultimately solvable problems in the control of a lower extremity exoskeleton. Some of those problems are briefly described as follows:

1. Depending on the architecture and design of the exoskeleton, one needs to install several force and torque sensors to measure all forces from the pilot on the exoskeleton because the pilot is in contact with the exoskeleton at several locations. These locations are not known in advance. For example, we have found that some pilots are interested in having braces connecting BLEEX at the shanks while some are interested in having them on the thighs. Inclusion of sensors on a leg to measure all kinds of human forces and torques

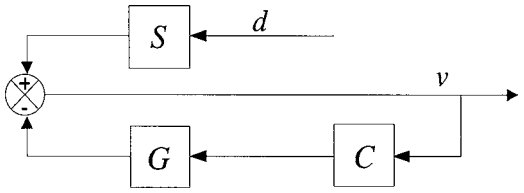

Fig. 4 Feedback control loop is added to block diagram of Fig. 3. *C* is the controller operating only on the exoskeleton variables.

may result in a system suitable for a laboratory setting but not robust enough to be deployed in the field.

2. If the BLEEX design is such that the forces and torques applied by the pilot on the exoskeleton are limited to a specified location (e.g., the pilot foot), then the sensor that measures the pilot forces and torques will also inadvertently measure other forces and torques that are not intended for locomotion. This is a major difference between measuring forces from, for example, the human hands and measuring forces from the human lower limbs. Using our hands, we are able to impose controlled forces and torques on upper extremity exoskeletons and haptic systems with very few uncertainties. However, our lower limbs have other primary and nonvoluntary functions, such as load support, that take priority over locomotion.
3. One option we have experimented with was the installation of sensing devices for forces on the bottom of the pilot's boots, where they are connected to BLEEX. Since the force on the bottom of the pilot's boot travels from heel to toe during normal walking, several sensors are required to measure the pilot force. Ideally, we would have a matrix of force sensors between the pilot and the exoskeleton feet to measure the pilot forces at all locations and at all directions. In practice, only a few sensors could be accommodated: at the toe, ball, midfoot, and the heel yet. This option has led to thick and bulky soles.
4. The bottoms of the human boots experience cyclic forces and torques during normal walking that lead to fatigue and eventual sensor failure if the sensor is not designed and isolated properly.

For the above reasons and our experience in the design of various lower extremity exoskeletons, it became evident that the existing state of technology in force sensing could not provide robust and repeatable measurement of the human lower limb force on the exoskeleton. Our goal then shifted to developing an exoskeleton with a large sensitivity to forces and torques from the operator using measurements only from the exoskeleton (i.e., no sensors on the pilot or the exoskeleton interface with the pilot). Creating a feedback loop only from the exoskeleton variables, as shown in Fig. 4, the new closed-loop sensitivity transfer function is

$$S_{\text{new}} = \frac{v}{d} = \frac{S}{1 + GC} \tag{2}$$

Observation of (2) reveals that $S_{\text{new}} \leqslant S$, and therefore any negative feedback from the exoskeleton, leads to an even smaller sensitivity transfer function. With respect to (2), our goal is to design a controller for a given S and G such that the closed-loop response from d to v (the new sensitivity function as given by (2)) is greater than the open-loop sensitivity transfer function (i.e., S) within some bounded frequency range. This design specification is given by inequality

$$|S_{\text{new}}| > |S| \quad \forall\, \omega \in (0, \omega_O) \tag{3}$$

or alternatively

$$|1 + GC| < 1 \quad \forall\, \omega \in (0, \omega_O) \tag{4}$$

where ω_O is the exoskeleton maneuvering bandwidth.

In classical and modern control theory, every effort is made to minimize the sensitivity function of a system to external forces and torques. But for exoskeleton control, one requires a totally opposite goal: *maximize the sensitivity of the closed-loop system to forces and torques*. In classical servo problems, negative feedback loops with large gains generally lead to small sensitivity within a bandwidth, which means that they reject forces and torques (usually called disturbances). However, the above analysis states that the exoskeleton controller needs a large sensitivity to forces and torques. From the perspective of the pilot, this has the effect making the exoskeleton feel and behave like a very small mass when the sensitivity of the closed-loop system to forces and torques is high.

To achieve a large sensitivity function, we use the inverse of the exoskeleton dynamics as a positive feedback controller so that the loop gain for the exoskeleton approaches unity (slightly less than 1). Assuming positive feedback, (2) can be written as

$$S_{\text{new}} = \frac{v}{d} = \frac{S}{1 - GC} \tag{5}$$

If C is chosen to be $C = 0.9G^{-1}$, then the new sensitivity transfer function is $S_{\text{new}} = 10S$ (ten times force amplification). In general, we recommend the use of positive feedback with a controller chosen as

$$C = (1 - \alpha^{-1})G^{-1} \tag{6}$$

where α is the amplification number greater than unity (for the above example, $\alpha = 10$ led to the choice of $C = 0.9G^{-1}$). Equation (6) simply states that a positive feedback controller needs to be chosen as the inverse dynamics of the system dynamics scaled down by $(1 - \alpha^{-1})$. Note that (6) prescribes the controller in the absence of unmodeled high-frequency exoskeleton dynamics. In practice, C also includes a unity gain low-pass filter to attenuate the unmodeled high-frequency exoskeleton dynamics.

The above method works well if the system model (i.e., G) is well known to the designer. If the model is not well known, then the system performance will differ greatly from the one predicted by (5), and in some cases instability will occur. The above simple solution comes with an expensive price: robustness to parameter variations. In order to get the above method working, one needs to know the dynamics of the system well. Section 3.2 discusses this trade-off.

3.2 Robustness to Parameter Variations. The variation in the new sensitivity transfer function when positive feedback is used is given by

$$\frac{\Delta S_{\text{new}}}{S_{\text{new}}} = \frac{\Delta S}{S} + \frac{GC}{1 - GC}\frac{\Delta G}{G} \tag{7}$$

If GC is close to unity (when the force amplification number α is large), any parameter variation on modeling will be amplified as well. For example, if the parameter uncertainty in the system is 10%, i.e.,

$$\left|\frac{\Delta G}{G}\right| = 0.10 \quad \text{and} \quad \left|\frac{\Delta S}{S}\right| = 0$$

then (7) results in

$$\left|\frac{\Delta S_{\text{new}}}{S_{\text{new}}}\right| = \left|\frac{GC}{1 - GC}\right| 0.10 \tag{8}$$

Now assume C is chosen such that $C = 0.9G^{-1}$. Substituting into (8) results in

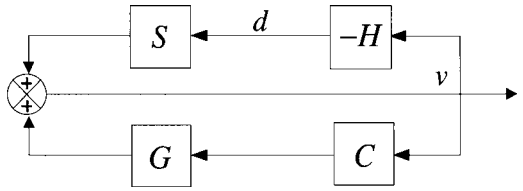

Fig. 5 This block diagram shows how an exoskeleton moves. The upper loop shows how its pilot moves the exoskeleton through applied forces. The lower loop shows how the controller drives the exoskeleton.

$$\left|\frac{\Delta S_{\text{new}}}{S_{\text{new}}}\right| = 0.90. \tag{9}$$

Equation (9) indicates that any parameter variation directly affects the system behavior. In the above example, a 10% error in model parameters results in nine times the variation in the sensitivity function. This is why model accuracy is crucial to exoskeleton control.

To get the above method working properly, one needs to understand the dynamics of the exoskeleton quite well, as the controller is heavily model based. One can see this problem as a trade-off: the design approach described above requires no sensor (e.g., force or EMG [20]) in the interface between the pilot and the exoskeleton; one can push and pull against the exoskeleton in any direction and at any location without measuring any variables on the interface. However, the control method requires a very good model of the system. At this time, our experiments with BLEEX have shown that this control scheme—which does not stabilize BLEEX—forces the exoskeleton to follow wide-bandwidth human maneuvers while carrying heavy loads. We have come to believe, to rephrase Friedrich Nietzsche, that *that which does not stabilize, will only make us stronger*.

3.3 Pilot Dynamics. There are many approaches to modeling the dynamics of a human, ranging from complete neuromusculoskeletal models [27,28] to a simplified spring damper representation. In particular, two types of human muscle modeling have been used successfully to provide insight into human dynamics. One is based on the investigation of the molecular or fiber range of the muscle, while the second is based on the relationship between the input and output properties of the muscle. See [29,30] for in-depth modeling and analysis. We have chosen the second approach and reported our preliminary work as applied to haptic systems and human power amplifiers.

In our control scheme, there is no need to include the internal components of the pilot limb model; the detailed dynamics of nerve conduction, muscle contraction, and central nervous system processing are implicitly accounted for in constructing the dynamic model of the pilot limbs. The pilot force on the exoskeleton, d, is a function of both the pilot dynamics H and the kinematics of the pilot limb (e.g., velocity, position, or a combination thereof). In general, H is determined primarily by the physical properties of the human dynamics. Here we assume H is a nonlinear operator representing the pilot impedance as a function of the pilot kinematics

$$d = -H(v) \tag{10}$$

The specific form of H is not known other than that it results in the human muscle force on the exoskeleton. Figure 5 represents the closed-loop system behavior when pilot dynamics is added to the block diagram of Fig. 4. Examining Fig. 5 reveals that (5), representing the new exoskeleton sensitivity function, is not affected by the feedback loop containing H.

Figure 5 shows an important characteristic for exoskeleton control. One can observe two feedback loops in the system. The upper feedback loop represents how forces and torques from the pilot affect the exoskeleton. The lower loop shows how the controlled feedback loop affects the exoskeleton. While the lower feedback loop is positive (potentially destabilizing), the upper feedback loop stabilizes the overall system of pilot and exoskeleton taken as a whole.

3.4 Effect of Pilot Dynamics on Closed-Loop Stability. How does the pilot's dynamic behavior affect the exoskeleton behavior? In order to get an understanding of the system behavior in the presence of pilot dynamics, we use our 1-DOF system and assume H is a linear transfer function. The stability of the system shown in Fig. 5 is decided by the closed-loop characteristic equation

$$1 + SH - GC = 0 \tag{11}$$

In the absence of feedback controller C, the pilot carries the entire load (payload plus the weight of the exoskeleton torso). The stability in this case is decided by the characteristic equation

$$1 + SH = 0 \tag{12}$$

Characteristic equation (12) is always stable since it represents the coupled pilot and exoskeleton behavior without any controller (i.e., when $GC=0$). Provided no neuromuscular control disorders exist, a human coupled to an entirely passive system is naturally stable. For example, if one were to holding a purely passive object, such as a pencil, there is little chance that the interaction with the object would become unstable. When feedback loop C is added, the closed-loop characteristic equation changes from (12) to (11), and using the small-gain theorem, one can show that the closed-loop stability is guaranteed as long as inequality (13) is satisfied

$$|GC| < |1 + SH| \quad \forall\, \omega \in (0,\infty) \tag{13}$$

According to (6), C is chosen such that $|GC|<1$, and therefore, in the absence of uncertainties, (13) is guaranteed as long as $1 \leqslant |1+SH|$. Unlike control methods utilized in the control of the upper extremity exoskeletons [21], the human dynamics in the control method described here has little potential to destabilize the system. Even though the feedback loop containing C is positive, the feedback loop containing H stabilizes the overall system of pilot and exoskeleton.

Example. For a 1-DOF system, $S=G=1/J_S$, v is angular velocity, J is the moment of inertia, and s is the Laplace operator. The human impedance is modeled as $H=M_H s+C_H$, where M_H and C_H are positive quantities. If $\alpha=10$ and the controller is chosen as $C=0.9Js$, the new sensitivity function is ten times larger than the original sensitivity function

$$S_{\text{new}} = \frac{v}{d} = \frac{S}{1 - GC} = 10S \tag{14}$$

The system characteristic equation when $C=0$ is given by (15) and always results in a stable system

$$1 + SH = \frac{(J + M_H)s + C_H}{Js} \tag{15}$$

The closed-loop characteristic equation when a positive feedback loop is used is given by (16) and also results in a stable system

$$1 + SH - GC = \frac{(0.1J + M_H)s + C_H}{Js} \tag{16}$$

Even if α is chosen as a larger number, the system in the absence of parameter uncertainties, is stable. Now suppose $\Delta J/J=-20\%$, i.e., $\Delta S/S=\Delta G/G=20\%$, then the variation in new sensitivity function is

$$\frac{\Delta S_{\text{new}}}{S_{\text{new}}} = \frac{\Delta S}{S} + \frac{GC}{1 - GC}\frac{\Delta G}{G} = 200\% \tag{17}$$

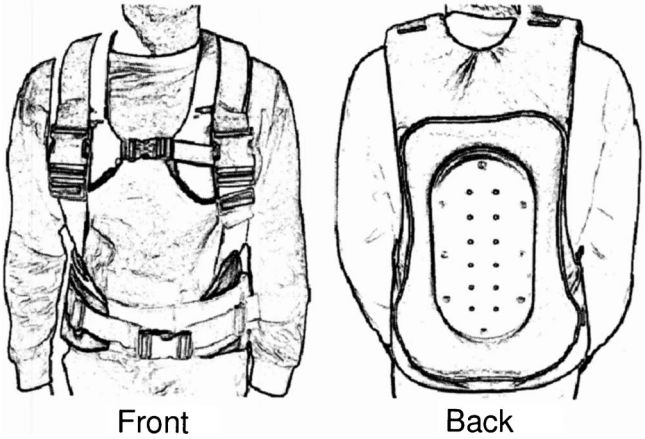

Fig. 6 The pilot vests shown here and in Fig. 1 are designed to uniformly distribute the BLEEX-pilot force on the pilot's upper body

In this case, $GC=(1/0.8Js)0.9Js=9/8$, $S=1/0.8Js$, and the closed-loop characteristic polynomial is represented by

$$1+SH-GC=\frac{(10M_H-J)s+10C_H}{8Js} \tag{18}$$

Equation (18) states that the system is unstable if $J>10M_H$. Thus, the system is vulnerable to model parameter uncertainties. In summary, the controller discussed here is stable when worn by the pilot as long as parameter uncertainties are kept to a minimum.

4 Implementation on BLEEX

The above discussion motivated the design philosophy using a 1-DOF system. BLEEX, as shown in Fig. 1, is a system with many degrees of freedom and therefore implementation of BLEEX control needs further attention. Each BLEEX leg has three degrees of freedom at the hip, one degree of freedom at the knee, and three degrees of freedom at the ankle. Both the flexion-extension and abduction-adduction degrees of freedom at the hip are actuated. The knee has one flexion-extension degree of freedom that is actuated. The ankle plantar/dorsi flexion (in the sagittal plane) is also actuated. The other three degrees of freedom (i.e., rotation and abduction-adduction at the ankle and rotation at the hip) are equipped with passive impedances using steel springs and elastomers. In summary, each BLEEX leg has four powered degrees of freedom: hip joint, knee joint, and ankle joint in the sagittal plane, and a hip abduction-adduction joint.

The pilot and BLEEX have rigid mechanical connections at the torso and the feet; everywhere else, the pilot and BLEEX have compliant or periodic contact. The connection at the torso is made using a vest, two variations of which can be seen in Fig. 1 and Fig. 6. One of the essential objectives in the design of these custom vests was to allow the distribution of the forces between BLEEX and the pilot, thereby preventing abrasion. These vests are made of several hard surfaces that are compliantly connected to each other using thick fabric. The adjustment mechanisms in the vests allow for a snug fit to the pilot. The vests include rigid plates (with hole patterns) on their backs for connection to the BLEEX torso.

The pilot's shoes or boots (Fig. 7(*a*)) attach to the BLEEX feet using a modified quick-release binding mechanism similar to snowboard bindings (Fig. 7(*b*)). A plate with the quick-release mechanism is attached to the rigid heel section of the BLEEX foot. Early versions of the BLEEX system had the pilot wearing a standard boot that has had a mating binding cleat secured to the heel. The cleat on the modified pilot boot does not interfere with normal wear when the pilot is unclipped from BLEEX. The BLEEX foot is composed of the rigid heel section with the binding mechanism and a compliant, but load bearing, toe section that begins at midfoot and extends to the toe. The BLEEX foot has a compressible rubber sole with a tread pattern that provides both shock absorption and traction while walking. The rubber sole of the BLEEX foot contains embedded sensors, as shown in Fig. 8 that detect the trajectory of the BLEEX-ground reaction force starting from heel-strike to toe-off. This information is used in the BLEEX controller to identify the BLEEX foot configuration relative to the ground.

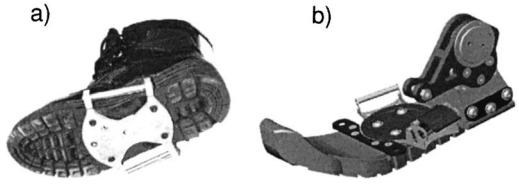

Fig. 7 Rigid attachment bindings between (*a*) the pilot boot and (*b*) the BLEEX foot

Although biomechanical studies of walking frequently identify seven or more distinct phases of the human walking gait cycle [31], for simplicity in control we consider BLEEX to have three distinct phases (shown in Fig. 9), which manifest to three different dynamic models:

1. Single support: One leg is in the stance configuration while another leg is in swing.
2. Double support: Both legs are in stance configuration and situated flat on the ground.
3. Double support with one redundancy: Both legs are in stance configuration, but one leg is situated flat on the ground while the other one is not.

Using the information from the sensors in the foot sole, the controller determines in which phase BLEEX is operating and which of the three dynamic models apply.

In our initial control design process, we decoupled the control of the abduction-adduction DOF at the hip from the control of joints in the sagittal plane. This is valid because we noted through measurements that the abduction-adduction movements during normal walking ($<$0.9 m/s or 2 mph) are rather small. In comparison to the movements in the sagittal plane, the abduction-adduction movements can be considered quasi-static maneuvers with little dynamical affects on the rest of system. This indicates that the exoskeleton dynamics in the sagittal plane are affected only by the abduction-adduction angle and not by the abduction-adduction dynamics. For the sake of brevity, Secs. 4.1–4.3 describe the control method in the sagittal plane for a given set of abduction-adduction angles.

4.1 Single Support. In the single-support phase, BLEEX is modeled as the 7-DOF serial link mechanism in the sagittal plane shown in Fig. 10. The inverse dynamics of BLEEX can be written in the general form as

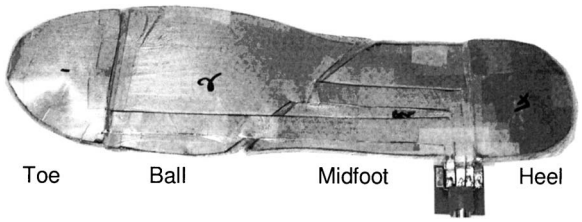

Fig. 8 The sensory system in one prototype BLEEX foot sole is composed of pressure sensitive semi-conductive rubber embedded in a polyurethane sole (Fig. 7(*b*)). This foot measures the ground reaction force profile at four locations: toe, ball, midfoot, and heel.

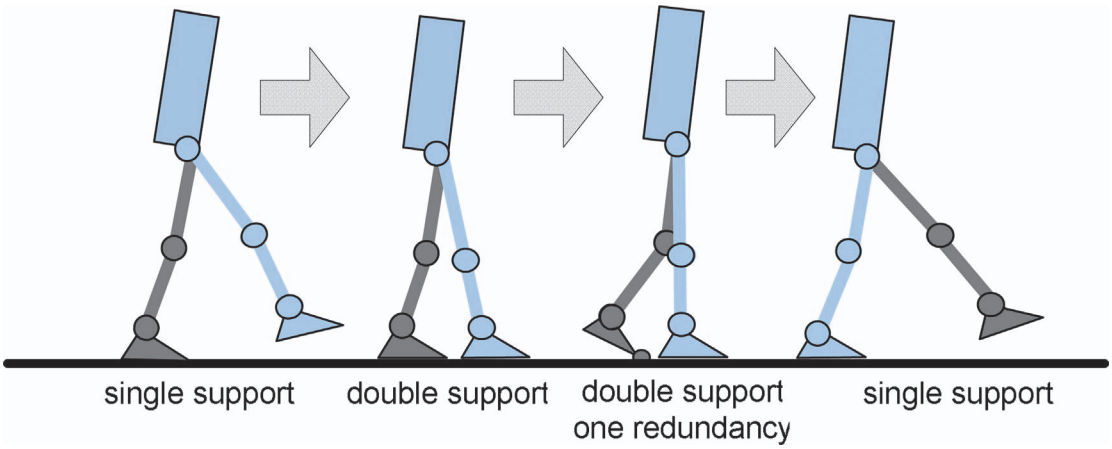

Fig. 9 Three phases of the BLEEX walking cycle

$$M(\theta)\ddot{\theta} + C(\theta,\dot{\theta})\dot{\theta} + P(\theta) = \mathbf{T} + \mathbf{d} \tag{19}$$

where $\theta=[\theta_1,\theta_2,\ldots,\theta_7]^T$ and $\mathbf{T}=[0,\mathbf{T}_1,\mathbf{T}_2,\ldots,\mathbf{T}_6]^T$.

M is a 7×7 inertia matrix and is a function of θ, $C(\theta,\dot{\theta})$ is a 7×7 centripetal and Coriolis matrix and is a function of θ and $\dot{\theta}$, and P is a 7×1 vector of gravitational torques and is a function of θ only. $\mathbf{T}$ is the 7×1 actuator torque vector with its first element set to zero since there is no actuator associated with joint angle θ_1 (i.e., angle between the BLEEX foot and the ground). $\mathbf{d}$ is the effective 7×1 torque vector imposed by the pilot on BLEEX at various locations. According to (6), we choose the controller to be the BLEEX inverse dynamics scaled by $(1-\alpha^{-1})$, where α is the amplification number.

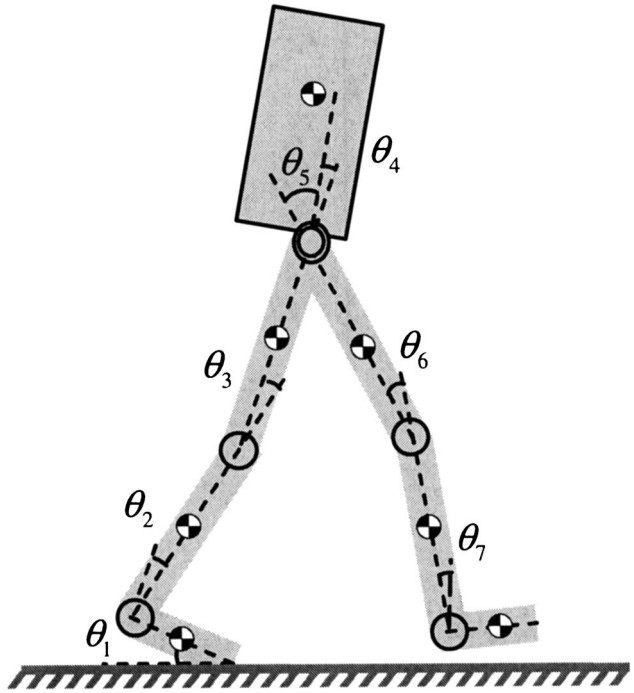

Fig. 10 Sagittal plane representation of BLEEX in the single-stance phase. The "torso" includes the combined exoskeleton torso mechanism, payload, control computer, and power source.

$$\mathbf{T} = \hat{P}(\theta) + (1-\alpha^{-1})[\hat{M}(\theta)\ddot{\theta} + \hat{C}(\theta,\dot{\theta})\dot{\theta}] \tag{20}$$

$\hat{C}(\theta,\dot{\theta})$, $\hat{P}(\theta)$, and $\hat{M}(\theta)$ are the estimates of the Coriolis matrix, gravity vector, and the inertia matrix, respectively, for the system shown in Fig. 10. Note that (20) results in a 7×1 actuator torque. Since there is no actuator between the BLEEX foot and the ground, the torque prescribed by the first element of $\mathbf{T}$ must be provided by the pilot. Substituting $\mathbf{T}$ from (20) into (19) yields

$$M(\theta)\ddot{\theta} + C(\theta,\dot{\theta})\dot{\theta} + P(\theta) = \hat{P}(\theta) + (1-\alpha^{-1})[\hat{M}(\theta)\ddot{\theta} + \hat{C}(\theta,\dot{\theta})\dot{\theta}] + \mathbf{d} \tag{21}$$

In the limit when $M(\theta)=\hat{M}(\theta)$, $C(\theta,\dot{\theta})=\hat{C}(\theta,\dot{\theta})$, $P(\theta)=\hat{P}(\theta)$, and α is sufficiently large, $\mathbf{d}$ will approach zero, meaning the pilot can walk as if BLEEX did not exist. However, it can be seen from (21) that the force felt by the pilot is a function of α and the accuracy of the estimates $\hat{C}(\theta,\dot{\theta})$, $\hat{P}(\theta)$, and $\hat{M}(\theta)$. In general, the more accurately the system is modeled, the less the human force d will be. In the presence of variations in abduction-adduction angles, only $P(\theta)$ in Eqs. (19) and (20) needs to be modified.

4.2 Double Support. In the double-support phase, both BLEEX feet are flat on the ground. The exoskeleton is modeled as two planar 3-DOF serial link mechanisms that are connected to each other along their uppermost link as shown in Fig. 11(*a*). The inverse dynamics for these serial links are represented by (22) and (23).

$$M_L(m_{TL},\theta_L)\ddot{\theta}_L + C_L(m_{TL},\dot{\theta}_L,\theta_L)\dot{\theta}_L + P_L(m_{TL},\theta_L) = \mathbf{T}_L + \mathbf{d}_L \tag{22}$$

$$M_R(m_{TR},\theta_R)\ddot{\theta}_R + C_R(m_{\mathbf{T}_R},\dot{\theta}_R,\theta_R)\dot{\theta}_R + P_R(m_{TR},\theta_R) = \mathbf{T}_R + \mathbf{d}_R \tag{23}$$

where $\theta_L=[\theta_{L1}\ \theta_{L2}\ \theta_{L3}]^T$ and $\theta_R=[\theta_{R1}\ \theta_{R2}\ \theta_{R3}]^T$. m_{TR} and m_{TL} are effective torso masses supported by each leg, and m_T is the total torso mass such that

$$m_T = m_{TR} + m_{TL} \tag{24}$$

The contributions of m_T on each leg (i.e., m_{TL} and m_{TR}) are chosen as functions of the location of the torso center of mass relative to the locations of the ankles such that

$$\frac{m_{TR}}{m_{TL}} = \frac{x_{TL}}{x_{TR}} \tag{25}$$

where x_{TL} is the horizontal distance between the torso center of mass and the left ankle and x_{TR} is the horizontal distance between the torso center of mass and the right ankle. For example, if the center of mass of the torso is located directly above the right leg,

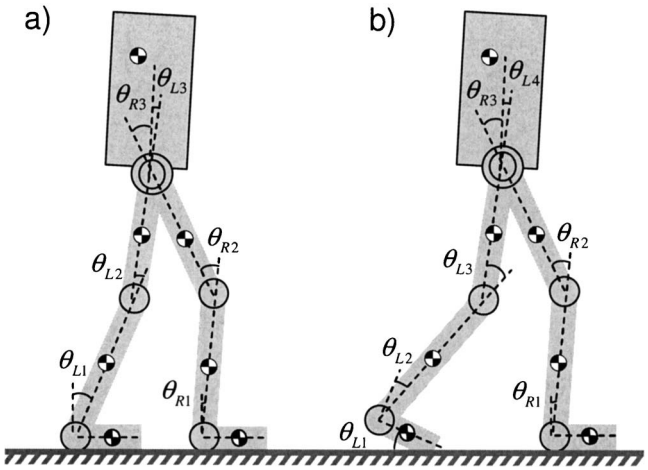

Fig. 11 Sagittal-plane representation of BLEEX in (*a*) the double-support phase and (*b*) the double-support phase with one redundancy

then $m_{TL}=0$ and $m_{TR}=m_T$. Similar to the single stance phase, the controllers are chosen such that

$$\mathbf{T}_L = \hat{P}_L(m_{TL},\theta_L) + (1-\alpha^{-1})[\hat{M}_L(m_{TL},\theta_L)\ddot{\theta}_L + \hat{C}_L(m_{TL},\theta_L,\dot{\theta}_L)\dot{\theta}_L] \tag{26}$$

$$\mathbf{T}_R = \hat{P}_R(m_{TR},\theta_R) + (1-\alpha^{-1})[\hat{M}_R(m_{TR},\theta_R)\ddot{\theta}_R + \hat{C}_R(m_{TR},\theta_R,\dot{\theta}_R)\dot{\theta}_R] \tag{27}$$

Needless-to-say, (25) is valid only for quasi-static conditions, where the accelerations and velocities are small. This is, in fact, the case, since in the double-support phase, both legs are on the ground and BLEEX's angular acceleration and velocities are quite small. This allows us to simplify (26) and (27) during slow walking by removing all terms except the estimates of the gravitational vectors.

4.3 Double Support With One Redundancy. Double support with one redundancy is modeled as a 3-DOF serial link mechanism for the stance leg with the foot flat on the ground and a 4-DOF serial link mechanism for the stance leg that is not completely on the ground (Fig. 11(*b*)). Each serial link supports a portion of the torso weight. The inverse dynamics for these serial links are represented by (28) and (29), where in the specific moment shown in Fig. 11(*b*), the left leg has four degrees of freedom and the right leg has three degrees of freedom.

$$M_L(m_{TL},\theta_L)\ddot{\theta}_L + C_L(m_{TL},\dot{\theta}_L,\theta_L)\dot{\theta}_L + P_L(m_{TL},\theta_L) = \mathbf{T}_L + \mathbf{d}_L \tag{28}$$

$$M_R(m_{TR},\theta_R)\ddot{\theta}_R + C_R(m_{TR},\dot{\theta}_R,\theta_R)\dot{\theta}_R + P_R(m_{TR},\theta_R) = \mathbf{T}_R + \mathbf{d}_R \tag{29}$$

where $\theta_L=[\theta_{L1}\ \theta_{L2}\ \theta_{L3}\ \theta_{L4}]^T$, $\theta_R=[\theta_{R1}\ \theta_{R2}\ \theta_{R3}]^T$, $\mathbf{T}_L=[0\ \mathbf{T}_{L1}\ \mathbf{T}_{L2}\ \mathbf{T}_{L3}]^T$, and $\mathbf{T}_R=[\mathbf{T}_{R1}\ \mathbf{T}_{R2}\ \mathbf{T}_{R3}]^T$. m_{TR} and m_{TL} are the effective torso masses supported by each leg and are computed similar to the double-support case by use of (25). Utilizing (28) and (29) as dynamic models of the exoskeleton, (26) and (27) are used as controllers in this case. Clearly, the actuator torque vector associated with the leg that has four degrees of freedom (e.g., $\mathbf{T}_L$ in the case shown in Fig. 11(*b*)) is a 4×1 vector. As in the single support phase, the torque prescribed by the first element of $\mathbf{T}$ must be provided by the pilot because there is no actuator between the BLEEX foot and the ground. As BLEEX goes through the various phases shown in Fig. 9, the sensors shown in Fig. 8 detect which leg has four degrees of freedom and which has three degrees of freedom. The controller then chooses the appropriate algorithm for each leg.

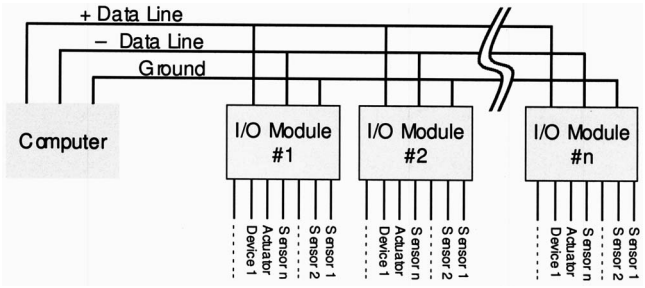

Fig. 12 The controller relies on a high-speed synchronous ring network topology where several remote input/output network nodes (shown as I/O Module #1) collect local sensor data and distribute local actuation commands

5 Control Implementation

Since all computations required to implement the control are conducted on a single computer, we needed a control platform to minimize the number of signal wires in the system. The exoskeleton electronics system, EXOLINK, was designed to simplify and reduce the cabling task of all the sensors and actuators needed for exoskeleton control. It relies on a high-speed synchronous ring network topology where several electronic remote input-output modules (RIOM) reside in a ring. Each RIOM is in communication with several sensors and one actuator in close proximity, and includes eight sixteen-bit analog-to-digital converters (ADC), two quadrature counters, eight bits of digital input and output ports, two digital-to-analog converters (DAC) and analog filters. Each RIOM also includes localized power regulation and isolation to minimize signal noise and system ground loops, and a built-in FPGA manages all RIOM data transaction and filtering. The data gathered by each module are encoded and transmitted digitally to a central computer through the ring. The EXOLINK has four rings, two of which are associated with the two legs. Each ring contains three remote input-output (I/O) modules (Fig. 12). A third ring is connected to a graphical user interface for debugging and data acquisition. A fourth ring is used to accommodate other electronic and communication gears which are not related to the exoskeleton but which the pilot may choose to carry. Each ring can accommodate up to eight RIOMs (Fig. 13). The EXOLINK consists of a microcomputer and a supervisor IO module (SIOM). The SIOM includes a FPGA programed to serve as the communication hub for all four rings. A transceiver chip residing in the SIOM and all the RIOMs allow for data transfer at a rate of 1500 Mb/s. Currently, a 650 MHz Pentium PC-104 form-factor microcomputer is used to implement the control algorithm, and the current exoskeleton utilizes 75% of the I/O capability of the EXOLINK. The use of a high-speed synchronous network in place of the traditional parallel method enables the exoskeleton to reduce the over 200 sensor and actuator wires to only 24 communication and power wires. While the sensors are read at the rate of 10 KHz, the control is updated at 4 KHz (control sampling time is 250 μs). The detailed implementation is described in [26].

6 Experimental Hardware

Fundamental to designing a lower extremity exoskeleton is selecting the overall structural architecture of the legs. Many different layouts of joints and limbs can combine to form a functioning leg. Regardless of whether linear sliders, rotary joints, or general compliancy are used to provide the necessary degrees of freedom, the architecture generally falls into one of a few categories.

6.1 Anthropomorphic. Anthropomorphic architectures attempt to exactly mirror the human leg. By kinematically matching the human, the exoskeleton's leg position follows the human leg's position. This greatly simplifies many design issues from avoiding human/machine collisions to predicting the required range of mo-

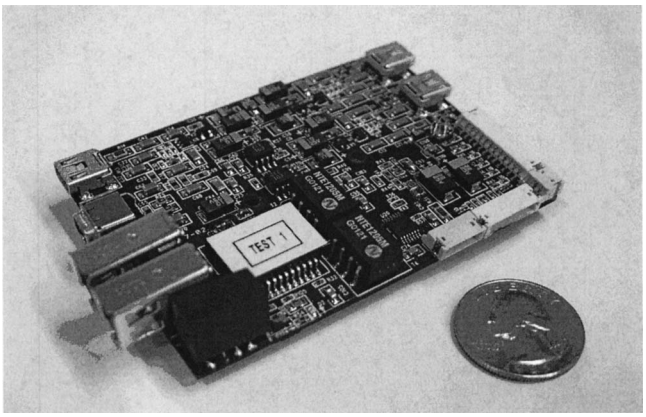

Fig. 13 Each RIOM (shown here) is in communication with several sensors and one actuator in close proximity

Table 1 Exoskeleton-joint ranges of motion. Exoskeleton flexibility must be less than the human flexibility limits for safety, but is kept close to the maximum human flexibility to maximize maneuverability.

	Human Walking Maximum [31]	Exoskeleton Maximum	Average Military Male Maximum [32]
Ankle Flexion	14.1°	45°	35°
Ankle Extension	20.6°	45°	38°
Ankle Abduction	not available	20°	23°
Ankle Adduction	not available	20°	24°
Knee Flexion	73.5°	121°	159°
Hip Flexion	32.2°	121°	125°
Hip Extension	22.5°	10°	not available
Hip Abduction	7.9°	16°	53°
Hip Adduction	6.4°	16°	31°
Total Medial Rotation	13.2°	35°	73°
Total Lateral Rotation	1.6°	35°	66°

tion for the robotic joints. However, many difficulties arrive when trying to match the human leg architecture. Major issues include matching the human's knee, which is more of a sliding joint than a pure rotary one. Also, for different operators to wear the exoskeleton, it must be highly adjustable to ensure that all of the exoskeleton joints align with the corresponding human joints. Anthropomorphic exoskeletons are a commonly seen architecture because it allows the exoskeleton to attach to the operator wherever desired.

6.2 Nonanthropomorphic. Although not as common in exoskeletons, many nonanthropomorphic devices are highly successful (e.g., bicycles). Nonanthropomorphic architectures open up a wide range of possibilities for the leg design as long as the exoskeleton never interferes with or limits the operator. Often it is difficult to develop architecture significantly different from a human leg that can still move the foot through all the necessary maneuvers (i.e. from turning tight corners to deep squats). Safety issues become more prominent with nonanthropomorphic designs because the exoskeleton must be absolutely prohibited from forcing the operator into a position he/she cannot reach. Even though anthropomorphic exoskeletons are more common, a clever nonanthropomorphic architecture could lead to simpler actuation or lower energy consumption.

6.3 Pseudoanthropomorphic. The BLEEX project chose an architecture that is almost anthropomorphic. If the exoskeleton kinematics are close to human kinematics, then appropriate ranges of motion for each degree of freedom can be easily approximated from human physiological data. Similar kinematics also make it

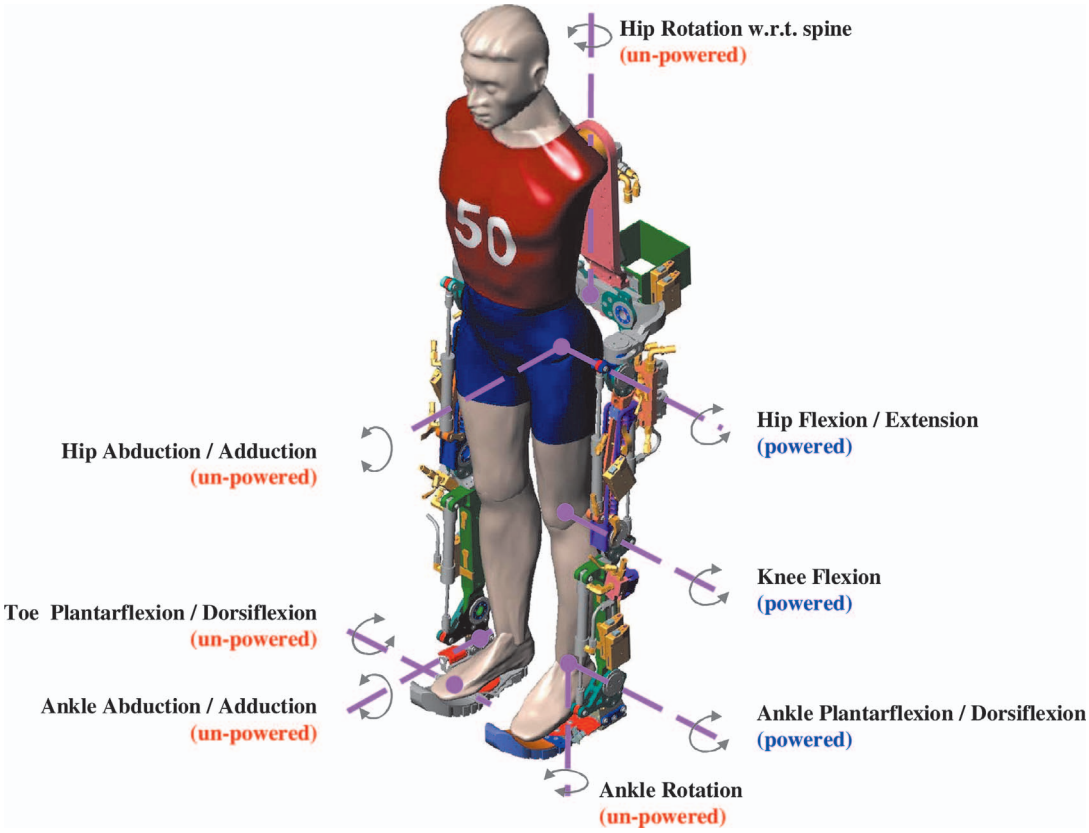

Fig. 14 BLEEX degrees of freedom

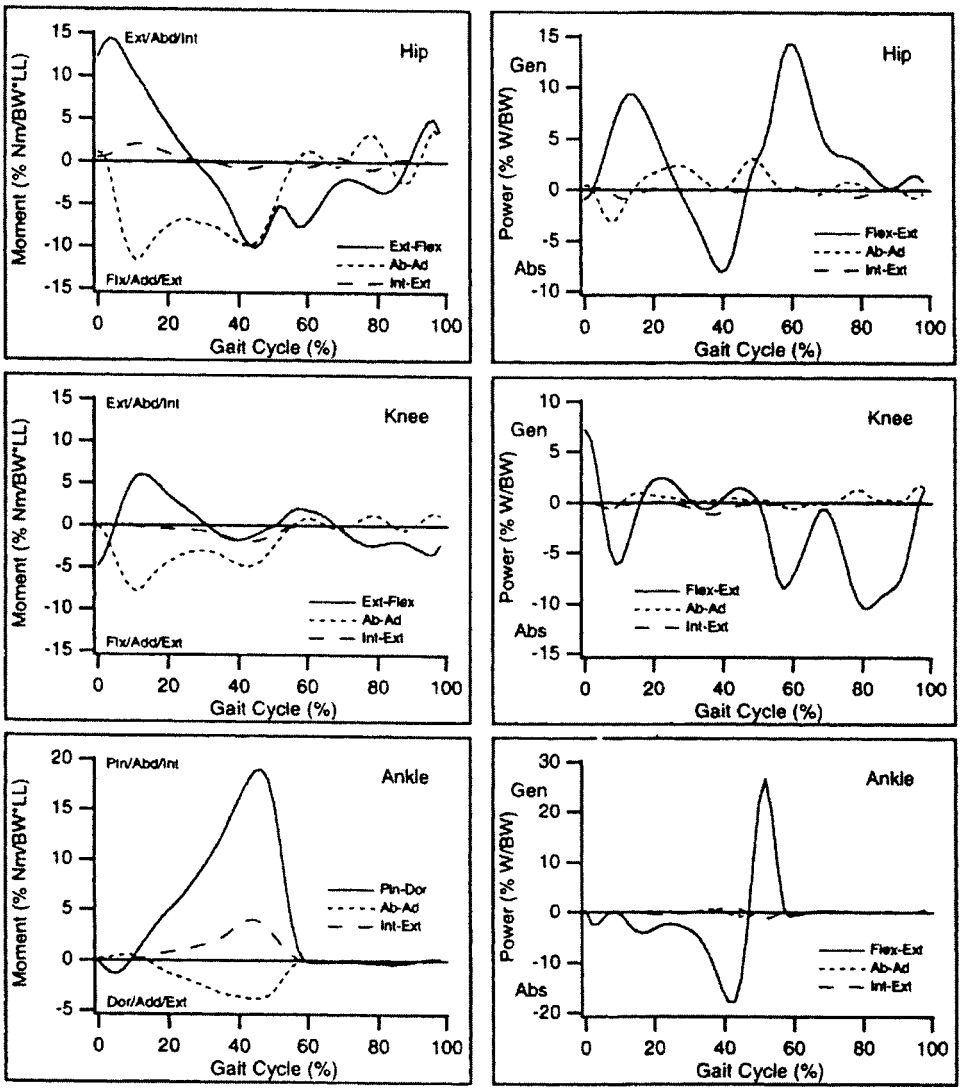

Fig. 15 Human power required for walking. The flexion/extension direction requires the most power for all three joints (ankle, knee, and hip). Besides these sagittal plane directions, the hip abduction/adduction requires the next most power [31].

easier for the exoskeleton to follow the human through any maneuver and not collide with the operator. However, attempting to exactly match human kinematics creates many design issues; thus, slight differences are tolerated for simplicity, such as approximating the knee as a pure rotary joint. Since the human and exoskeleton leg kinematics are not exactly the same, the human and machine are only rigidly connected at the extremities of the exoskeleton (feet and torso). Any other rigid connections would lead to large forces imposed on the operator due to the kinematic differences. However, compliant connections along the leg are tolerable as long as they allow relative motion between the human and machine. If the inertias and masses of the exoskeleton leg segments are similar to the corresponding human limbs, then the desired joint torques for the exoskeleton can be estimated using human clinical gait analysis (CGA) data [1]. Using a pseudoanthropomorphic architecture, the exoskeleton is much easier to size for various operators and the joint ranges of motion and torques are approximately equal to those of a human, but the rigid connections points are limited to just the feet and torso.

6.4 Degrees of Freedom. Since the BLEEX has a pseudoanthropomorphic architecture, its degrees of freedom need to approximately match a human. Thus, like a human, the exoskeleton has a hip, knee, and ankle. Generally, the exoskeleton kinematics are modeled exactly after the human, but the exoskeleton degrees of freedom include a few key simplifications.

First, the exoskeleton knee joint is simplified to a pure rotary joint. A human knee joint is a complex combination of rolling and sliding between the femur and tibia that allows the joint's center of rotation to move as the knee bends [31]. Using a pure rotary joint at the knee simplifies the design and dynamic model of the exoskeleton, but will cause the exoskeleton knee to not exactly mirror the human knee. Also, the moving center of rotation of the human knee plays an important role in helping the leg slightly hyperextend to an over-center configuration. This function will be absent in the exoskeleton knee and that compromise should be acknowledged.

Another kinematic simplification in the exoskeleton is the leg rotation. A human's leg can rotate a small amount at many different locations: the hip joint, knee joint, along the shank, and in the ankle joint [32]. To keep the functionality of these motions, but simplify the design, the exoskeleton rotation is condensed to joints at the hip and ankle.

Initially, the three degrees of freedom at the hip were designed to be collocated and aligned with the human's hip joint. However,

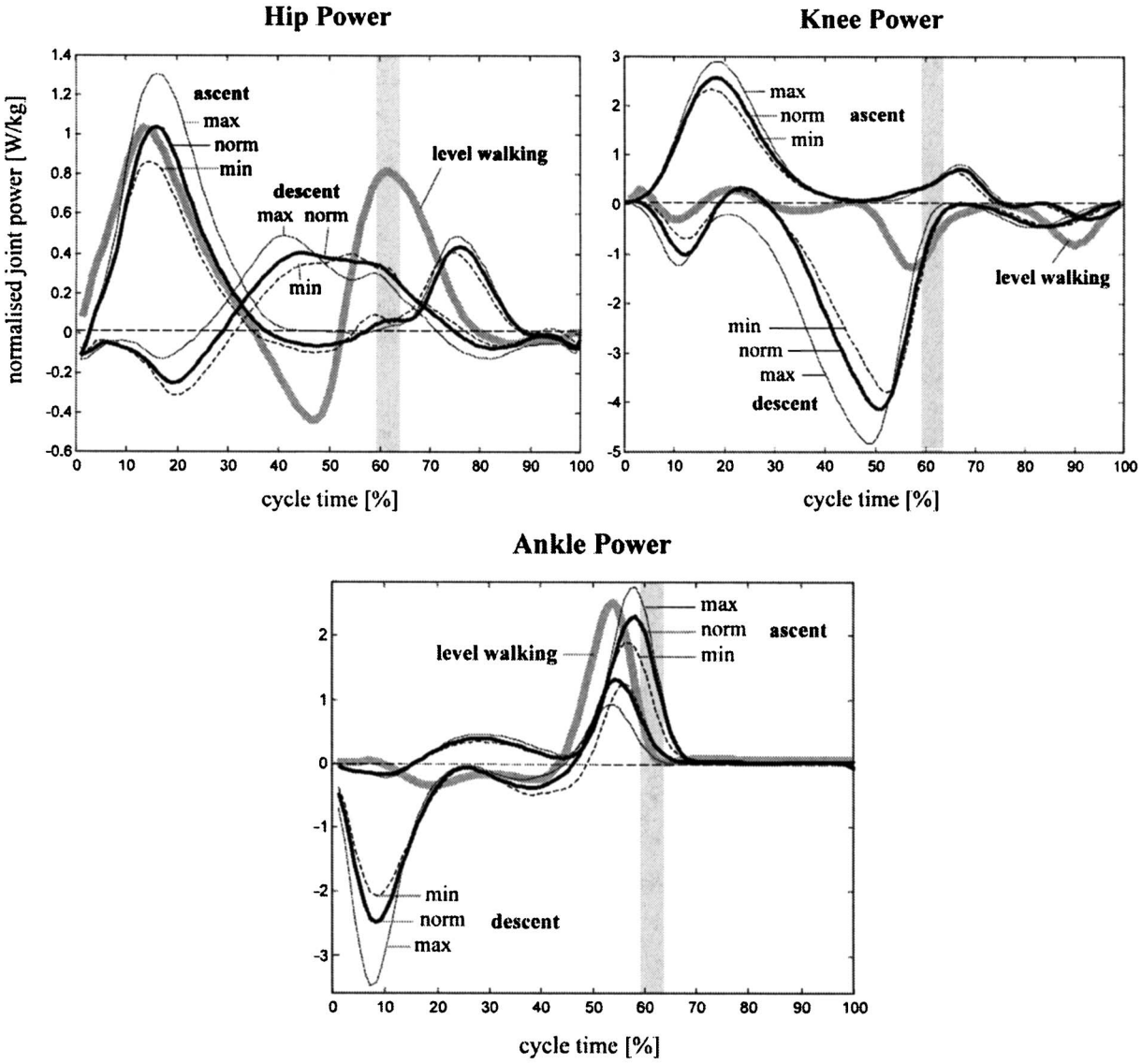

Fig. 16 Power required for ascending/descending Stairs. The knee requires power when ascending stairs instead of absorbing power as it does during level walking [35].

all these designs significantly limited the hip rotation because of mechanical interference of the hip linkages with themselves or the human. Therefore, the rotation was moved such that it no longer aligns with the human's rotation. Kinematically, the exoskeleton leg has sufficient degrees of freedom to account for the misalignment. Similar allowances were made at the ankle, where the abduction and rotation axes do not align with the human's axes of rotation.

With these simplifications, the exoskeleton has seven degrees of freedom per leg (Fig. 14):

- three degrees of freedom at the hip
- one degree of freedom at the knee (pure rotation in the sagittal plane)
- three degrees of freedom at the ankle

An additional degree of freedom is added to the exoskeleton foot. The front of the exoskeleton foot, under the human's toes, is compliant. This allows the exoskeleton foot to flex with the human's foot as they get up on their toes.

6.5 Range of Motion. The BLEEX kinematics are similar to human leg kinematics; thus, the motion limits for each of the exoskeleton joints is determined by examining human-joint ranges of motion. At the very least, the exoskeleton must be able to shadow the human through a normal walking motion. CGA data reveal the angles of each joint during walking and, thus, the minimum range of motion for each joint [30]. Safety dictates that the exoskeleton should not have motion limits greater than the operator. Therefore, the maximum range of motion for each joint is determined by the human's maximum flexibility [32]. Ideally, all the joint ranges of motion would be slightly smaller than the limits of human flexibility to prevent injury but allow maximum maneuverability of the exoskeleton. However, as discussed, linear actuators are used in BLEEX, which limits some of the joint ranges of motion. Joints, such as the knee, have a reduced flexibility to prevent the actuator from reaching singularity. Other limits on the joints' motion were determined through prototype testing. For example, the ankle plantar-dorsi flexion limits are outside the normal human flexibility. Mock-up testing indicated that this additional flexibility is necessary for full maneuverability

since the human's foot is not held completely rigid relative to the exoskeleton foot Table 1 shows the exoskeleton-joint ranges of motion.

6.6 Which Joints to Actuate? Each exoskeleton leg has seven degrees of freedom (eight counting the toe flexibility), but arbitrarily deciding to actuate all of them leads to unnecessarily high power consumption and control complexity. Instead, a minimum number of joints necessary to maintain functionality should be actuated. For the exoskeleton to be functional, the human operator should only move the exoskeleton and payload with a minimum amount of power. Therefore, any degrees of freedom requiring a substantial amount of power should be actuated, or limited by another impedance. For this first generation of BLEEX, actuation was designed primarily for walking; thus, once again, CGA data were used to determine which degrees of freedom consumed power while walking.

As expected, CGA data show that the highest amount of power is used for flexion and extension at the ankle, knee, and hip [30,31,33,34] (Fig. 15). The ankle and hip both require significant positive power and, thus, need to be actuated. The knee mainly requires negative power (it absorbs power) while walking; thus, it could be controlled with damper. Even though the actuation is mainly designed for level walking, when walking up steps, an incline, or squatting, the knee becomes a very critical joint for adding positive power to the system [35] (Fig. 16). Therefore, the knee joint is also actuated. Besides flexion and extension, hip abduction/adduction requires the most power for walking because it provides the lateral balancing forces. To help with the lateral balancing and maneuverability, the hip abduction of BLEEX is actuated. According to CGA data, the other degrees of freedom all have very small power consumptions while walking and, thus, remain unactuated.

7 Conclusion

Although there is still significant work to be done before the project is complete, BLEEX has successfully walked, carrying its own weight and producing its own power. This makes it the first lower extremity exoskeleton capable of carrying a payload and being energetically autonomous. Currently, BLEEX has been demonstrated to support up to 70 kg (exoskeleton weight plus payload), walk at speeds up to 1.3 m/s, and shadow the operator through most maneuvers without any human sensing or preprogramed motions. BLEEX is not a typical servomechanism. While providing disturbance rejection along some axes preventing motion in response to gravitational forces, BLEEX actually encourages motion along other axes in response to pilot interface forces. This characteristic requires large sensitivity to pilot forces, which invalidates certain assumptions of the standard control design methodologies and, thus, requires a new design approach. The controller described here uses the inverse dynamics of the exoskeleton as a positive feedback controller so that the loop gain for the exoskeleton approaches unity (slightly less than 1). Our current experiments with BLEEX have shown that this control scheme has two superior characteristics: (i) it allows for the same wide bandwidth maneuvers a human is capable of performing and (ii) it is unaffected by changing human dynamics (i.e., no changes to the controller are required when pilots are switched). The tradeoff is that it requires a relatively accurate model of the system. A body local area network to host the control algorithm is developed in [25]. Video clips that demonstrate the effectiveness of this control scheme can be found at http://bleex.me.berkeley.edu/bleex.htm.

References

[1] Chu, A., Kazerooni, H., and Zoss, A., 2005, "On the Biomimetic Design of the Berkeley Lower Extremity Exoskeleton (BLEEX)," IEEE Int. Conf. on Robotics and Automation, April, Barcelona.

[2] Kazerooni, H., Racine, J.-L., Huang, L., and Steger, R., 2005, "On the Control of the Berkeley Lower Extremity Exoskeleton (BLEEX)," IEEE Int. Conf. on Robotics and Automation, April, Barcelona.

[3] Zoss, A., and Kazerooni, H., 2005, "On the Mechanical Design of the Berkeley Lower Extremity Exoskeleton," IEEE Intelligent Robots and Systems Conference, August, Edmunton.

[4] Kazerooni, H., 1990, "Human-Robot Interaction via the Transfer of Power and Information Signals," IEEE Trans. Syst. Man Cybern., **20**(2), pp. 450–463.

[5] Kazerooni, H., and Guo, J., 1993, "Human Extenders," ASME J. Dyn. Syst., Meas., Control, **115**(2B), pp. 281–289.

[6] Kazerooni, H., and Mahoney, S., 1991, "Dynamics and Control of Robotic Systems Worn By Humans," ASME J. Dyn. Syst., Meas., Control, **113**(3), pp. 379–387.

[7] Kazerooni, H., and Her, M., 1994, "The Dynamics and Control of a Haptic Interface Device," IEEE Trans. Rob. Autom., **10**(4), pp. 453–464.

[8] Kazerooni, H., and Snyder, T., 1995, "A Case Study on Dynamics of Haptic Devices: Human Induced Instability in Powered Hand Controllers," J. Guid. Control Dyn., **18**(1), pp. 108–113.

[9] Mizen, N. J., 1965, "Preliminary Design for the Shoulders and Arms of a Powered, Exoskeletal Structure," Cornell Aeronautical Laboratory Report No. VO-1692-V-4.

[10] Groshaw, P. F., General Electric Co., 1969, "Hardiman I Arm Test, Hardiman I Prototype," General Electric, Schenectady, NY, Report No. S-70-1019.

[11] General Electric Co., 1968, "Hardiman I Prototype Project, Special Interim Study," General Electric Schenectady, NY, Report No. S-68-1060.

[12] Makinson, B. J., General Electric Co., 1971, "Research and Development Prototype for Machine Augmentation of Human Strength and Endurance, Hardiman I Project," General Electric, Schenectady, NY, Report No. S-71-1056.

[13] Mosher, R. S., 1960, "Force-Reflecting Electrohydraulic Manipulator," Electro-Technol., pp. 138–141.

[14] Vukobratovic, M., Hristic, D., and Stojiljkovic, Z., 1974, "Development of Active Anthropomorphic Exoskeleton,"Med. Biol. Eng., **12**, pp. 66–80.

[15] Vukobratovic, M., Ciric, V., and Hristic, D., 1972, "Contribution to the Study of Active Exoskeletons," *Proc. of the 5th IFAC Congress*, Paris.

[16] Hirai, K., Hirose, M., Haikawa, Y., and Takenaka, T., 1998, "The Development of Honda Humanoid Robot," *Proc. of the 1998 IEEE International Conference on Robotics & Automation*, Leuven, Belgium, IEEE, New York, pp. 1321–1326.

[17] Colombo, G., Jorg, M., and Dietz, V., 2000, "Driven Gait Orthosis to do Locomotor Training of Paraplegic Patients," 22nd Annual International Conf. of the IEEE-EMBS, Chicago, July 23–28.

[18] Pratt, J., Krupp, B., Morse, C., and Collins, S., 2004, "The RoboKnee: An Exoskeleton for Enhancing Strength and Endurance During Walking," IEEE Intl. Conf. on Robotics and Automation, New Orleans.

[19] Kawamoto, H., Kanbe, S., and Sankai, Y., 2003, "Power Assist Method for HAL-3 Estimating Operator's Intention Based on Motion Information," *Proc. of 2003 IEEE Workshop on Robot and Human Interactive Communication*, Millbrae, CA, IEEE, New York, pp. 67–72.

[20] Kawamoto, H., and Sankai, Y., 2002, "Power Assist System HAL-3 for gait Disorder Person," ICCHP, July, Austria.

[21] Kazerooni, H., 1996, "The Human Power Amplifier Technology at the University of California, Berkeley," Int. J. Rob. Autom., **19**, pp. 179–187.

[22] McGee, T., Raade, J., and Kazerooni, H., 2004, "Monopropellant-Driven Free Piston Hydraulic Pump for Mobile Robotic Systems," ASME J. Dyn. Syst., Meas., Control, **126**(1), pp. 75–81.

[23] Raade, J., and Kazerooni, H., 2005, "Analysis and Design of a Novel Power Source for Mobile Robots," IEEE. Trans. Autom. Sci. Eng., **2**(3), pp. 226–232.

[24] Amundsen, K., Raade, J., Harding, N., and Kazerooni, H., 2005, "Hybrid Hydraulic-Electric Power Unit for Field and Service Robots," IEEE Intelligent Robots and Systems Conference, August, Edmunton.

[25] Kim, S., Anwar, G., and Kazerooni, H., 2004, "High-Speed Communication Network for Controls With Application on the Exoskeleton," American Control Conference, Boston, June.

[26] Kim, S., and Kazerooni, H., 2004, "High Speed Ring-Based Distributed Networked Control System for Real-Time Multivariable Applications," ASME International Mechanical Engineering Congress, Anaheim, November.

[27] Berstein, N. A., 1967, *The Control and Regulation of Movements*, Pergamon Press, London.

[28] Bizzi, E., Hogan, N., Mussa-Ivaldi, F. A., and Giszter, S., 1992, "Does the Nervous System Use Equilibrium Point Control to Guide Single and Multiple Joint Movements?," Behav. Brain Sci., **15**, pp. 603–613.

[29] Wilkie, D. R., 1950, "The Relation Between Force and Velocity in Human Muscle," J. Physiol. (London), **K110**, pp. 248–280.

[30] Winters, J. M., and Stark, L., 1985, "Analysis of Fundamental Human Movement Patterns Through the Use on In-Depth Antagonistic Muscle Models," IEEE Trans. Biomed. Eng., **BME32**(10), pp. 826–839.

[31] Rose, J., and Gamble, J. G., 1994, *Human Walking*, 2nd ed., Williams & Wilkins, Baltimore, p. 26.

[32] Woodson, W., Tillman, B., and Tillman, P., 1992, *Human Factors Design Handbook*, McGraw-Hill, New York, pp. 550–552.

[33] Kirtley, C., 2005, "CGA Normative Gait Database: Hong Kong Polytechnic University, 10 Young Adults," Accessed August, http://guardian.curtin.edu.au/cga/data/.

[34] Linskell, J., "CGA Normative Gait Database: Limb Fitting Centre, Dundee, Scotland, Young Adult," Available at http://guardian.curtin.edu.au/cga/data/.

[35] Riener, R., Rabuffetti, M., and Frigo, C., 2002, "Stair Ascent and Descent at Different Inclinations," Gait and Posture, **15**, pp. 32–34.